Detailed Atmosphere Model Fits to Disk-Dominated ULX Spectra

Yawei Hui, Julian H. Krolik

Department of Physics and Astronomy, Johns Hopkins University, Baltimore, MD 21218;
ywhui@pha.jhu.edu, jhk@pha.jhu.edu

ABSTRACT

We have chosen 6 Ultra-Luminous X-ray sources from the *XMM-Newton* archive whose spectra have high signal-to-noise and can be fitted solely with a disk model without requiring any power-law component. To estimate systematic errors in the inferred parameters, we fit every spectrum to two different disk models, one based on local blackbody emission (KERRBB) and one based on detailed atmosphere modelling (BHSPEC). Both incorporate full general relativistic treatment of the disk surface brightness profile, photon Doppler shifts, and photon trajectories. We found in every case that they give almost identical fits and similar acceptable parameters. The best-fit value of the most interesting parameter, the mass of the central object, is between 23 and 73 $M_\odot$ in 5 of the 6 examples. In every case, the best-fit inclination angle and mass are correlated, in the sense that large mass corresponds to high inclination. Even after allowing for this degeneracy, we find that, with $\gtrsim 99.9\%$ formal statistical confidence, 3 of the 6 objects have mass $\gtrsim 25\ M_\odot$; for the other 3, these data are consistent with a wide range of masses. A mass greater than several hundred $M_\odot$ is unlikely for the 3 best-constrained objects. These fits also suggest comparatively rapid black hole spin in the 3 objects whose masses are relatively well-determined, but our estimate of the spin is subject to significant systematic error having to do with uncertainty in the underlying surface brightness profile.

Subject headings: black hole physics – accretion disk – IMBH – X-ray

1. Introduction

Nearly two decades since their first unveiling in the X-ray sky (Fabbiano & Trinchieri 1987), Ultra-Luminous X-ray sources (ULXs) still remain puzzles. The X-ray luminosities of these off-galaxy-center point sources fall in the range $10^{39} - 10^{41}$ erg s^{-1} in the $2 - 10$ keV band, at least an order of magnitude larger than those of Galactic X-ray Binaries (GXB) and

several orders of magnitude smaller than those of Active Galactic Nuclei (AGN). If ULXs are accreting black hole systems that observe the Eddington limit ($L_E = 1.3 \times 10^{38}$ erg s^{-1}), the central black holes must have masses from a few tens to a few thousands of solar masses, i.e. they must be intermediate mass black holes (IMBH). Some evidence has been found in support of this view (see Colbert & Mushotzky 1999; Miller & Hamilton 2002; Miller et al. 2003). But it is also possible that ULXs' masses are smaller than the Eddington limit suggests. They might be stellar mass black holes whose radiation is beamed in the observed direction (King et al. 2001) or which are accreting at super-Eddington rates (Begelman 2002, 2006; Stern & Poutanen 2006). The only way to distinguish between these scenarios is to measure the central masses of ULXs as accurately as possible.

The most reliable way to measure the masses of the stars in a binary is to observe their orbital motions. Unfortunately, this method does not work in the context of ULXs. Because there are so far no clearly identified spectral lines in ULXs' spectra, the common technique used in spectroscopic binaries cannot be applied. Temporal variability is another approach. After comparing the Fourier power spectra of GXBs and AGNs, some researchers (e.g. McHardy et al. (2006)) have concluded that the characteristic timescales of accreting black holes are proportional to their central objects' masses. If ULXs are extragalactic analogs to the GXB systems in our galaxy, similar correlations between quasi-periodic oscillation (QPO) frequencies and mass may be used to estimate ULX masses. These correlations have been established successfully for several ULXs, for example, M82 X1 (Strohmayer & Mushotzky 2003) and NGC 5408 X1 (Strohmayer et al. 2007). The discovery of the QPO in NGC 5408 X1 led to an estimated ULX mass of $1500 - 3500$ M$_\odot$. However, these works treated a limited number of ULXs and it is not guaranteed that QPOs can be found in a large sample of ULXs. Even if there is a QPO identified in the power spectrum of a ULX, the mass inferred through this method is highly dependent on the "calibration standard" and may be quite uncertain (see, for example Strohmayer et al. 2007).

Another method for inferring the central mass is spectral fitting (Vierdayanti et al. 2006; Winter et al. 2006, 2007). To fit a ULX spectrum, various models and/or model combinations can be exploited. In practice, ULXs' spectra are usually modelled by a combination of a thermal disk component and a power-law (Miller et al. 2003, 2004; Roberts et al. 2004)). In this combination, the thermal disk component covers the soft X-ray ($0.3 - 1$ or 2 keV) range of the spectrum while the power-law takes care of the hard tail ($1 - 10$ keV and above). Because the spectrum of soft X-ray radiation from the accretion disk is dependent on the central mass, but there is no clear relation between the hard tail of the spectrum and the central mass, we define our sample to include exclusively those ULXs with only thermal disk components in their spectra. In this way, we can focus purely on the component of the system — the thermal accretion disk — with the tightest connection to the central object's

mass, as well as the other key accretion parameters: spin, accretion rate and inclination angle.

There are many thermal disk models that have been used in this way. In Xspec11, for instance, there are DISKBB, DISKPN, GRAD, KERRBB. These models share more or less the same core — the multi-color disk (MCD) approximation (Mitsuda et al. 1984; Makishima et al. 1986; Shimura & Takahara 1995). In this approximation, one assumes that the disk emission is a sum of a series of local blackbody spectra with effective temperatures defined by the standard disk model but modified by a hardening factor. The version we employ here is KERRBB, which also incorporates general relativistic effects. Even though the MCD approximation works well in the case of GXB (Davis et al. 2005), in this paper, we also fit the data to a model in which a detailed stellar atmosphere is computed for each disk annulus. Our reason to do so is that earlier work (Hui et al. 2005) has shown that the spectral shape, especially around the peak energy, can be altered by atomic features when the central mass is larger than typical stellar masses (> 100 M$_\odot$). This model (which also fully includes general relativistic effects) has been compiled to an easy-to-use table model in Xspec11 (BHSPEC: Davis & Hubeny (2006)); we modified it and extended its parameter space to cover a wider range of central masses (see § 4 for details).

In § 2 we describe the sample selection criteria and in § 3 the data reduction procedure. The disk model BHSPEC is briefly discussed, and specific fitting results for each object are presented in § 4. For comparison, previous work on the objects in our sample is briefly described in § 5. We discuss our results in § 6 and draw conclusions in § 7.

2. Sample selection — disk dominated ULXs

Our sample was drawn from the *XMM-Newton* public data archive. We began with the object lists compiled by Winter et. al. (see Table 6 in Winter et al. (2006) and Table 1 in Winter et al. (2007)). For their sample, Winter et al. chose objects observed for at least 10 ks and with distance less than 8 Mpc. These criteria guaranteed a minimum of 400 counts for objects with $L_X > 2 \times 10^{38}$ erg s^{-1}. To focus on ULX candidates, they also removed all objects with spectra distinctly different (e.g., resembling supernova remnants) and all objects located at the centers of their host galaxies (to eliminate AGN). We chose those ULX candidates with > 1000 counts in order to guarantee good signal-to-noise in the reduced spectra. Then, in order to retain as much as possible of the soft X-ray emission from the accretion disk, we excluded those objects with neutral hydrogen column density in the line of sight larger than 10^{22} cm^{-2} as determined by Winter et al. (see Table 4 in Winter et al. (2006) and Table 2 in Winter et al. (2007)), except for Circinus X1 and X2,

which have slightly higher values. There are 23 objects meeting these criteria.

We then used the latest version (7.0) of the *XMM-Newton* Science Analysis System (SAS) and calibration (up to date as of Jan. 2007) to reprocess the data and obtain the event files. After applying proper filters (see § 3 for details), source and background spectra for each of these objects were created and fitted by the "disk+powlaw" combination in Xspec11. Specifically, we used a photoelectric absorption model (phabs) to account for the opacity in the interstellar medium and the thermal disk model BHSPEC (a detailed disk model discussed later in this paper) plus a power-law component. To decide which model component (disk or powlaw) dominates the spectral output, we computed the integrated counts from both components and defined the spectrum to be dominated by one or the other when one component contributes more than 70% of the total counts. There are 11 powlaw-dominated spectra, 6 disk+powlaw spectra, and only 6 objects (see Table 1) having disk-dominated spectra. In other words, we can use the disk model alone to fit those 6 disk-dominated spectra. In these objects, a non-zero power-law contribution at best marginally improves the quality of the fit and sometimes even harms it.

3. Data reduction

We used the latest version (7.0) of SAS and the up-to-date calibration (Jan. 2007) to reprocess the Observation Data Files (ODF). Commands "emchain" (for EPIC-MOS) and "epchain" (for EPIC-PN) in SAS 7.0 were used to get the new processed pipeline products (PPS) which include the photon event files. Standard data filter procedures were followed according to the instructions in the *XMM-Newton* ABC guide. Good events were required to satisfy the following conditions: 1) for the MOS (both MOS1 and MOS2) detectors, the event pattern is in the 0 to 12 range (single, double, triple, and quadruple pixel events) and the pulse height is in the range of 0.2 – 12 keV; 2) for the PN detector, the event pattern is in the 0 to 4 range (single and double pixel events) and the pulse height is in the range of 0.2 – 15 keV. The #XMMEA_EM (for the MOS) filter and #XMMEA_EP (for the PN) filter were also applied together with a "FLAG==0" filter to kick out any bad or close-to-edge events captured by the CCDs. The light curve for each observation was produced with the SAS command 'evselect" to decide a proper time filtering threshold in order to reduce the influence from high rate flaring. For the MOS detectors, the good time intervals were selected by setting the rate to less than 5 cts s^{-1} (sometimes a little bit higher); for the PN detector, the threshold varies from 25 to 60 cts s^{-1}.

After obtaining the filtered event files, source and background spectra were extracted by using the SAS procedure "especget". For the sources, circular regions with radii of 20

arcseconds (± 10 according to the size of the sources and closeness to other sources or detector edges) were applied in the spectra extraction. For the background, a nearby circular region close to but without overlap on the source's region was used, with radius double the size of its corresponding source. SAS procedures "rmfgen" and "arfgen" were used to generate the response matrix files (RMF) and ancillary response files (ARF). Finally, we used the command in HEASOFT 6.1 — "grppha" — to regroup the spectra so that there are at least 20 photon counts in every spectral bin.

4. Model description and fitting results

4.1. BHSPEC vs KERRBB

We fitted the selected spectra with both BHSPEC (a detailed atmosphere calculation) and KERRBB (a MCD model). For details of KERRBB, see Li et al. (2005) and the Xspec11 manual; the only significant choice we made was to set the dilution factor to 1.7. BHSPEC is based on an atmosphere model of a standard $\alpha-$disk (Shakura & Sunyaev 1973) where each ring is treated in hydrostatic equilibrium and energy balance. The stress parameter α is chosen to be 0.01 so that all disk annuli are optically thick. The radiation intensity is computed as a function of both frequency and position by means of a full radiation transfer solution. Continuum opacities due to free electrons, H, He, C, N, O, Ne, Mg, Si, S, Ar, Ca, Fe and Ni, with the abundances given by Anders & Grevesse (1989) are calculated on the basis of explicit ionization balance calculations and statistical equilibrium of the most populated internal states. Photon-electron energy exchange by Comptonization is also included in the transfer solution. General relativity effects in photon propagation are taken into account: radiation is boosted and beamed, and its trajectories "bent" in the general relativistic potential before it reaches infinity (Agol 1997). For further details, see Hui et al. (2005).

In the work of Davis & Hubeny (2006), disks with many black hole masses, spins, accretion rates, and inclination angles were modelled, and the spectra obtained were compiled into the Xspec11 table model BHSPEC. For this project, we extended the parameter space considered by Davis and Hubeny to include disks around black holes with masses in the range of $10 - 10^4$ M$_\odot$. Because the internal consistency of disk models becomes dubious when the luminosity approaches or exceeds the Eddington luminosity, we included no models with $L/L_E > 1$. When we speak of lower bounds on the mass based on BHSPEC-fitting, we therefore always mean that this bound is subject to the constraint of being consistent with a disk model, i.e., keeping the luminosity sub-Eddington. It should be borne in mind, however, that some significant flexibility nonetheless remains at the low-mass end of parameter space

because altering the inclination angle or the black hole rotation rate could keep the luminosity in our direction at the level required by the measurements even while the luminosity in other directions is diminished in order to satisfy the sub-Eddington constraint. We did not so restrict KERRBB, so any super-Eddington fits it produces must be regarded as extremely suspect because the underlying model would then be inappropriate. For technical reasons, we limited the range of spins considered by BHSPEC to $0 \leq a/M \leq 0.997$ and by KERRBB to $-0.999 \leq a/M \leq 0.999$.

4.2. Fitting results

The fitting results for the objects in our sample are shown in Table 2. Each object is given two rows. The first row, with the object's name, describes the fit with BHSPEC; the second row shows the result from KERRBB. In BHSPEC, the normalization is fixed at a value corresponding to the best estimate for that object's distance (tabulated in Table 1). All other parameters, i.e., the equivalent hydrogen column density of photoelectric absorption, the black hole mass and spin, the accretion rate, and the disk viewing angle are set free to vary. In KERRBB, the parameter "distance" is fixed to the same value as in BHSPEC for each object and the normalization is set to 1.0. KERRBB also offers several other parameters. We freeze "eta" to zero (the zero torque inner boundary condition), "hd" to 1.7 (common diluted black body spectrum), "rflag" to -1.0 (self-irradiation is off), and "lflag" to 1.0 (limb-darkening is on).

The best-fit values and their uncertainties are shown in Table 2. All are statistically acceptable, and in each case the BHSPEC least χ^2 is slightly smaller than the KERRBB value. All one-parameter uncertainties were computed with $\Delta\chi^2 = 2.706$, equivalent to 90% confidence for a single parameter. For the BHSPEC fits, besides the best values, we also calculated the ratio of the observed luminosity ($E = 0.3 - 10$ keV, except for Circinus X2 MOS1, in which case the integration is limited in $E = 0.55 - 10$ keV) to the computed total intrinsic luminosity ($E = 0 - \infty$ keV) emitted in our direction; these are shown in the last column of Table 2. The fact that all these ratios are close to unity demonstrates that the *XMM-Newton* energy band contains nearly all the light our models suggest is being radiated.

In the case of KERRBB, the spectral fitting gives the accretion rate in the form of $\dot{M}$ instead of the dimensionless L/L_E. We used the following formula to translate between those two definitions, assuming that the radiative efficiency, η, is the standard function of a/M (Novikov & Thorne 1973).

$$\frac{L}{L_E} = \frac{\eta \dot{M} c^2}{1.3 \times 10^{38} M}.$$

Here c is the speed of light, $\dot{M}$ is the accretion rate in units of gm s^{-1} and M is the accretor's mass in units of M$_\odot$. Because the total luminosity of an object is fixed when the distance is known, the ratio L/L_E is actually inversely proportional to the object's mass. For this reason, only the uncertainty in the estimated mass is taken into account in the quoted uncertainty for L/L_E.

In the following subsections, we discuss each object individually. The spectra and best-fit models (BHSPEC only) are shown in the multipanel Figure 1. The KERRBB fits are so nearly identical to the BHSPEC fits that figures displaying them would be visually indistinguishable from each other.

4.2.1. M81 X1

We used a 120 ks *XMM-Newton* observation (0200980101) of Holmberg IX (made in September 2004) for M81 X1, which appears in the same field. We extracted spectra from the event files generated for the MOS1 and MOS2 cameras and fitted them with BHSPEC and KERRBB. The mass of the black hole is inferred to be $67 - 85$ M$_\odot$ from BHSPEC, while KERRBB gives a partially overlapping, but rather wider possible range, $33 - 74$ M$_\odot$. For the accretion rate, both BHSPEC and KERRBB indicate values close to the Eddington limit, which makes the applicability of both models suspect because both assume thin disks. Both models also give similar values for the hydrogen column density ($1.5 - 2.0 \times 10^{21}$ cm^{-2}), the black hole spin (close to the maximum Kerr value) and inclination angle ($50°$ - $70°$).

4.2.2. M101 X2

M101 was observed (0104260101) in June 2002 for a duration of 43 ks. We extracted spectra for the MOS1, MOS2 and PN cameras. The BHSPEC fit suggests that the black hole in M101 X2 has a mass $30 - 178$ M$_\odot$ and the spin of the black hole is close to the maximum Kerr value. The accretion rate may be anywhere from the Eddington limit down to a moderate level ($L/L_E \simeq 0.3$). The viewing angle is inferred to be $42° - 78°$. Using KERRBB indicates a lower hydrogen column density and larger uncertainty ranges for the mass and accretion rate even though the best-fit values are not far from those found using BHSPEC. The spin and the viewing angle in the KERRBB fit are totally unbounded.

4.2.3. NGC 253 X1, X3 and X4

The observation (0152020101) of NGC 253 was made in June 2003 with a duration of 140 ks. The spectra were drawn from the event files of the MOS1, MOS2 and PN cameras.

For NGC 253 X1, both BHSPEC and KERRBB indicate similar hydrogen column densities. For the black hole mass, BHSPEC infers a 90% confidence range of $50 - 81$ M$_\odot$, while KERRBB gives a very similar, but slightly wider range, $54 - 95$ M$_\odot$. In both models, the spin is quite large and very close to the maximum Kerr value. The Eddington-normalized luminosity inferred by BHSPEC is $0.35 < L/L_E < 0.56$, while KERRBB suggests a lower range, $0.18 < L/L_E < 0.31$. The viewing angle is well constrained by both models in the range $64°$ - $83°$.

In the case of NGC 253 X3, the uncertainty in the black hole mass derived from both BHSPEC and KERRBB is somewhat greater, from 25 to 80 M$_\odot$ for BHSPEC, from 32 to 176 M$_\odot$ for KERRBB. In terms of L/L_E, the range preferred by BHSPEC (L/L_E from 0.13 to 0.39) overlaps that of KERRBB (L/L_E from 0.03 to 0.18), but for the most part suggests higher values. Both models give their best fits when the black hole spins rapidly. The viewing angle is large, estimated to be between $44°$ and $85°$.

The inferred black hole mass from BHSPEC for NGC 253 X4 lies in the range $10 - 91$ M$_\odot$; KERRBB gives a similarly large uncertainty, from $5 - 77$ M$_\odot$. For the normalized luminosity, the two models have different best-fit values ($L/L_E = 0.14$ for BHSPEC and 0.05 for KERRBB), but the ranges permitted within the errors overlap to a considerable extent: $0.06 - 0.24$ (BHSPEC) and $0.02 - 0.35$ (KERRBB). BHSPEC suggests rapid black hole spin with a large viewing angle ($43° - 88°$), while KERRBB puts no constraint on either of these two parameters.

4.2.4. Circinus X2

Circinus X2 was observed (0111240101) in August 2001 for a duration of 110 ks. We extracted its spectra for both the MOS1 and PN cameras. Both BHSPEC and KERRBB failed to constrain almost all parameters except the hydrogen column density ($5.0 - 5.9 \times 10^{21}$ cm^{-2}). Unlike the other objects in our sample, the best-fit values of the mass inferred by BHSPEC and KERRBB (i.e., 340 M$_\odot$ vs. 13 M$_\odot$) are quite different, while the best-fit values of $\cos i$ are also very different (0.07 vs 1.00). This apparent conflict will be addressed later in the discussion when we investigate the correlation between inferred mass and inclination angle.

5.   Comparison to previous work

In a thorough study of M81 X1 (there named M81 X6) based on a May 2000 observation by *Chandra*, Swartz et al. (2003) (hereafter, S2003) showed that the best-fit model for the reduced spectrum is an absorbed disk blackbody. This disk domination in the spectrum is confirmed in our study. Swartz et. al. found the hydrogen column density (in units of 10^{21} cm^{-1}) to be 2.17 ± 0.10, which is close to our fitting results, $1.91^{+0.12}_{-0.11}$ for BHSPEC and $1.61^{+0.11}_{-0.11}$ for KERRBB. The black hole mass they estimated was 18 M$_\odot$, but they did so assuming the black hole is non-rotating. According to our fitting results (for both BHSPEC and KERRBB), the spin of the black hole in M81 X1 has close to the maximum Kerr value. These results are compatible with our estimate that the mass is $33 - 85$ M$_\odot$ because the (Boyer-Lindquist) radial coordinate of the innermost stable circular orbit (ISCO) for a maximal Kerr BH is $\simeq \frac{1}{6}$ that of a Schwarzschild BH of the same mass.

In S2003 and a previous *ASCA* study of M81 X1 (Makishima et al. 2000), the total luminosities were reported to be equal to or even exceeding the Eddington limits of the inferred black hole masses. To avoid this violation of conventional expectations, a bigger black hole mass (to give a higher Eddington limit) with a larger spin (to make a smaller ISCO) was suggested by some authors. As shown by our results, however, if one is constrained by fitting the spectrum, there is a limit to how much the mass and spin can be increased, and neither our atmosphere-based spectral model nor the multi-color disk model is consistent with substantially sub-Eddington behavior.

Jenkins et al. (2004) studied the same *XMM-Newton* observation of the galaxy M101 as we did, but named M101 X2 M101 XMM-1. They fitted the spectrum with a single disk component (DISKBB in Xspec) with satisfactory statistics and obtained an inner disk temperature ($T_{in} = 1.33$ keV). Due to the limited predictive power of DISKBB, no further conclusions were reached in their work.

6.   Discussion

Before dealing with our principal concern, the inferred masses of these objects, we first discuss a more technical point: the surprising lack of difference between BHSPEC and KERRBB when fitting the spectra. As described in § 4.1, BHSPEC is a much more sophisticated model than KERRBB and one might expect that the atomic features it can predict might lead to interestingly different fitting results. The fundamental reason why this does not happen is that, at the color temperatures of the objects in our sample, even Fe is fully-stripped. It is worth elaborating briefly on this point because this constraint

enters in a somewhat indirect fashion. To zeroth order, the temperature of the disk scales as $L^{1/4}M^{-1/2}$. If there were no relativistic Doppler shifts, the color temperature and luminosity would then suffice to determine the mass. However, disks around black holes do offer large Doppler factors, opening a wider parameter space in which to search for acceptable models. For these objects, we find that in part of this parameter space, the mass is high enough ($\gtrsim 100$ M$_\odot$) that the temperature in the disk drops to the point where the unstripped fraction of the heaviest abundant elements can produce an interesting level of opacity in atomic features (Davis & Hubeny 2006; Hui et al. 2005). However, the very fact that the fluid-frame temperature is this low means that, in order for the spectrum generated to fit the data, it must be Doppler boosted, which always implies large inclination angle, and can be enhanced by rapid black hole spin. However, the non-uniformity of the boost around the disk surface also entails strong smearing of sharp features. The result is that atomic features are never apparent in any of our fits, even in the extreme case of Circinus X2, in which the best-fit mass is 340 M$_\odot$. Moreover, because the unstripped ion fractions are so small at thermodynamic temperatures close to the observed color temperatures, this conclusion is only very weakly dependent upon elemental abundances. There is however, one possible exception to these arguments: in the presence of some atomic opacity, the error entailed in KERRBB by assuming a Planckian output spectrum with a fixed dilution factor may be larger than in a case in which there is truly zero atomic opacity.

We now turn to the main goal of this project: our attempt to use spectral fitting of thermal disk spectra to constrain the masses of ULXs. In Figure 2, we plot the best-fit values and uncertainties of the black hole masses for all our objects except Circinus X2. As that figure shows, the best-fit values of the black hole masses span a surprisingly small range, between 20 and 80 M$_\odot$. In fact, the error bars are large enough that the fits are consistent with all five having the same mass, $\simeq 75 \pm 10$ M$_\odot$.

Moreover, this range appears to be quite different from that seen in Galactic black hole binaries. As reviewed by McClintock & Remillard (2004), of all 17 GXBs with measured black hole masses, there are none in which the mass is likely to be smaller than 3 M$_\odot$ or larger than 18 M$_\odot$.

However, before we can conclude that these objects have a distinctly different mass distribution than the Galactic black holes, it is important to look more closely at the dominant source of uncertainty in the mass: the degeneracy between M and $\cos i$. Sun & Malkan (1989) pointed out that these two quantities are related almost inversely. In their disk fitting analysis of quasars and Seyfert galaxies, they found

$$\log(M) \propto -b\cos i,$$

where b is a parameter that varies between 0.6 (for $a/M = 0$) and $\simeq 1.2$ (for $a/M = 0.998$).

The origin of this relationship lies in the fact that higher inclination produces greater blue-shifting of light from matter orbiting toward us, thus compensating for the diminution of temperature that generally occurs with larger central mass (and therefore radiating area). The coefficient is a function of spin because the orbital speed near and outside the ISCO increases with more rapid rotation.

We find a very similar degeneracy in our fits. It is illustrated in the multipanel Figure 3. These figures plot the confidence level contours obtained from fitting to the BHSPEC model as seen in the M – $\cos i$ plane embedded in the higher-dimensional χ^2 parameter space. The value of χ^2 as a function of M and $\cos i$ is found by minimizing χ^2 over all the other parameters for those two values of mass and inclination. There is indeed a correlation between the mass and the inclination angle for every object. In addition, two dashed lines in the figures show the slope of the Sun & Malkan (1989) relations, the steeper one for maximal spin, the shallower one for no black hole spin. In most cases, as one might expect, their slopes bracket the slope of the correlation.

This degeneracy explains the large contrast between the BHSPEC and KERRBB best-fit masses for Circinus X2. In the former case, the best fit has $\cos i \simeq 0$ and $M \simeq 340$ M$_\odot$, while in the latter, $\cos i \simeq 1$ and $M \simeq 13$ M$_\odot$. Nonetheless, in terms of the BHSPEC fitting, these two very different answers differ statistically by only $1 - 2\sigma$.

With this degeneracy in mind, we now return to evaluating the fitting results for the other five objects in our sample. If one assumes a disk model, three of these — M81 X1, M101 X2, and NGC 253 X1 — require relatively large masses, in all three cases > 25 M$_\odot$. Smaller masses would lead to very large χ^2, no matter what other parameters (spin, inclination angle, intervening column density) are chosen. At the same time, the fits also suggest that their masses are not extremely large, generally $\lesssim 150 - 300$ M$_\odot$. Regrettably, however, our confidence that the formally best constrained of these (M81 X1) has a large mass must be tempered by the realization that the L/L_E implied by even the highest acceptable mass for this object is $\simeq 0.85$, a normalized luminosity so large as to call into question the physical standing of the model from which it was derived.

It is also of interest that the three objects with the strongest lower bound on the inferred mass are exactly the three objects in our sample with the greatest luminosity, from $\simeq 3 - 8 \times 10^{39}$ erg s^{-1}. Although M101 X2 and NGC 253 X1 do not have inferred luminosities in Eddington units as high as that of M81 X1, they are not far below: $\simeq 0.3 - 1$ for M101 X2 and $\simeq 0.35 - 0.55$ for NGC 253 X1.

The remaining two (NGC 253 X3 and X4) have best-fit masses that are several tens of solar masses, but their data are also consistent with a mass both considerably lower

($\lesssim 10$ M$_\odot$) and considerably higher ($\gtrsim 100$ M$_\odot$). Circinus X2, as we have already discussed, is also in this category, but with an even wider range of uncertainty. All three of these have luminosities low enough, $3 - 10 \times 10^{38}$ erg s^{-1}, that they are at best borderline ULXs in any case.

Along with the mass and inclination angle, our fits are also sensitive to the black hole rotation rate. Viewed in the mass–spin plane, χ^2 rises sharply in the case of the three best-constrained objects, M 81, M 101, and NGC 253 X-1 when $a/M \lesssim 0.8$–0.9. There is a slight degeneracy between these two variables, in the sense that lower spin requires smaller mass, but it is quite weak. However, we do not regard these results as robust because of a potential systematic error: our assumption of a Novikov-Thorne surface brightness profile.

If, as recent work on MHD stresses in accretion disks suggests (Krolik et al. 2005), there are significant stresses throughout the region of marginally stable (or even unstable) orbits, additional dissipation there is also likely. The result would be, for fixed luminosity, a shift to higher temperature and a smaller effective radiating area in the emitted spectrum (Agol & Krolik 2000). Employing an estimate of the local dissipation rate derived from simulation data and a general relativistic ray-tracing code to find what portion of the radiation reaches infinity, Beckwith et al. (2008) have recently computed the effective "radiation edge" due to these effects. They found that when $a/M \lesssim 0.9$ and the inclination angle is such that $\cos i \lesssim 0.7$, the characteristic radius for the radiation seen by distant observers can be displaced inward by factors of several relative to the prediction of the Novikov-Thorne model.

The sense of the bias induced by fitting a spectrum on the basis of a Novikov-Thorne surface brightness profile if the radiation edge really is located closer to the black hole is to find a mass smaller and/or a spin larger than the actual one. A factor of 2 error in the characteristic radius in gravitational units (i.e., r/r_g) translates directly into a factor of 2 in mass because $r_g = GM/c^2$. In terms of spin, a factor of 2 error would mean that a nominal best-fit of $a/M = 0.9$ should be reinterpreted as actually indicating $a/M = 0.4$ if the true radiation edge, like the radiation edge predicted by the Novikov-Thorne model, scales linearly with the radius of marginal stability.

Given the several order of magnitude *a priori* uncertainty in our knowledge of the masses of ULXs, a factor of 2 systematic error in mass is, at this stage, not a major handicap. Moreover, because we are especially concerned with determining whether ULX black hole masses can be as small as those found in Galactic black hole binaries, the fact that any correction would *increase* the inferred black hole mass means that the Novikov-Thorne estimate is a conservative one.

On the other hand, given the much more limited range of possible black hole rotation rates, a systematic error of order unity is a major concern in this context. In addition, the character of the spectral fitting acts to enhance the magnitude of the possible systematic error. Diminishing the spin in a model fit, by moving the radiation edge outward, also lowers the characteristic temperature for fixed luminosity and black hole mass. In order for the spectrum that results to fit the data, a larger orbital blue shift is required, forcing the model toward greater inclination angle. Large inclination angles are exactly where Beckwith et al. (2008) found the largest offsets between the radiation edge as predicted by the Novikov-Thorne model and the edge as inferred from simulation data.

7. Summary

After selecting the 23 known ULXs with the highest signal-to-noise and least absorbing column density, we chose a subsample of 6 objects in which the spectrum appeared to be purely that of a thermal disk, with no hint of any power-law component. Fitting their spectra with two different disk models (one based on the multi-color disk approximation, the other resting on detailed stellar atmosphere calculations), we found that in all but one case, the results were very similar: the masses yielding the best fits to the data lie between 20 and 80 $M_\odot$. In the exception, the two models suggested very different masses, 340 $M_\odot$ in the case of the atmosphere model, 13 $M_\odot$ in the case of the multi-color disk model.

More significantly, in 3 of the 6, the model fitting (that is, a search for those parameters for which a disk model can reproduce the observed spectrum to within the errors) formally excludes masses similar to those seen in Galactic black holes, ~ 10 $M_\odot$. The models clearly prefer rather larger masses, from several tens of solar masses to ~ 100 $M_\odot$, although in one case the value of L/L_E preferred by the model-fitting is so large ($\simeq 1$) as to be physically inconsistent with a disk model. We also see formal upper bounds on the mass that are generally $\simeq 150 - 300$ $M_\odot$, although systematic error having to do with the detailed surface brightness profile of relativistic disks may relax these bounds by a factor of $2 - 3$. In the other three objects, the error bars are too broad to permit confident exclusion of either conventionally small masses or considerably larger ones.

On this basis, we believe that these data provide significant new evidence that at least some ULXs have masses rather greater — $\simeq 30 - 100$ $M_\odot$ — than is found in ordinary Galactic binary black holes.

about the calculation of disk atmospheres. We especially acknowledge Ivan Hubeny for construction and maintenance of the stellar atmosphere code TLUSTY and its disk version TLUSDISK.

REFERENCES

Agol, E. 1997, Ph.D dissertation

Agol, E., & Krolik, J. H. 2000, ApJ, 507, 304

Anders, E., & Grevesse, N. 1989, Geochim. Cosmochim. Acta, 53, 197

Beckwith, K., Hawley, J. F. & Krolik, J. H. 2008, astro-ph/0801.2974, submitted to MNRAS

Begelman, M. C., 2002, ApJ, 568, L97

Begelman, M. C., 2006, ApJ, 643, 1065

Colbert, E. J. M., & Mushotzky, R. F. 1999, ApJ, 519, 89

Davis, S. W., Blaes, O. M., Hubeny, I., & Turner, N. J. 2004, ApJ, 621, 372

Davis, S. W., & Hubeny, I. 2006, ApJS, 164,530

Fabbiano, G., & Trinchieri, G. 1987, ApJ, 315, 46

Freeman, K. C., Karlsson, B., Lynga, G., Burrell, J. F., van Woerden, H., Goss, W. M. & Mebold, U. 1977, A&A, 55, 445

Freedman, W. L. & et. al. 1994, ApJ, 427, 628

Hui, Y. W., Krolik, J. H., & Hubeny, I. 2005, ApJ, 625, 913H

Iaria, R., Spanó, , M,; Di Salvo, T., Robba, N. R., Burderi, L., Fender, R., van der Klis, M., Frontera, F. 2005, ApJ, 619, 503

Jenkins, L. P., Roberts, T. P., Warwick, R. S. & Kilgard, R. E. 2004, MNRAS, 349, 404

Jurcevic, J. S. & Butcher, D. 2006, AAS Meeting 208, Bulletin of the American Astronomical Society, Vol. 38, p.92

Karachentsev, I. D., Grebel, E. K., Sharina, M. E., Dolphin, A. E., Geisler, D., Guhathakurta, P., Hodge, P. W., Karachentseva, V. E., Sarajedini, A. & Seitzer, P. 2003, A&A, 404, 93K

Kelson, D. D. & et. al. 1996, ApJ, 463, 26

King, A. R., Davies, M. B., Ward, M. J., Fabbiano, G., & Elvis, M. 2001, ApJ, 552, L109

Krolik, J. H., Hawley, J. F. & Hirose, S. 2005, ApJ, 622, 1008

Li, L. X., Zimmerman, E. R., Narayan, R., & McClintock, J. E. 2005, ApJS, 157, 335

Makishima, K., et al 1986, ApJ, 308, 635

Makishima, K., et al 2000, ApJ, 535, 632

McClintock J. E. & Remillard R. A. 2004, in Compact Stellar X-Ray Sources, eds. W. H. G. Lewin & M. van der Klis (Cambridge: Cambridge Univ. Press)

McHardy, I. M., Koerding, E., Knigge, C., Uttley, P., & Fender, R. P. 2006, Nature, 444, 730

Millis, M. C., & Hamilton, D. P. 2002, MNRAS, 330, 232

Miller, J. M., Fabbiano, G., Miller, M. C., & Fabian, A. C. 2003, ApJ, 585, L37

Miller, J. M., Fabian, A. C., & Miller, M. C. 2004, ApJ, 607, 931

Mitsuda, K. et al 1984, PASJ, 36, 741

Novikov, I. D., & Thorne, K. S. 1973, in Black Holes, eds. C. De Witt& B. De Witt (New York: Gordon and Breach), 343

Rekola, R., Richer, M. G., McCall, M. L., Valtonen, M. J., Kotilainen, J. K. & Flynn, C. 2005, MNRAS, 361, 330

Roberts, T. P., Warwick, R. S., Ward, M. J., & Goad, M. R. 2004, MNRAS, 349, 1193R

Shakura, N. I., Sunyaev, R. A. 1973, A&A, 24, 337

Shimura, T., Takahara, F. 1995, ApJ, 445, 780

Stern, B. E., & Poutanen, J. 2006, MNRAS, 372, 1217

Strohmayer, T. E. & Mushotzky, R. F. 2003, ApJ, 586, L61

Strohmayer, T. E. Mushotzky, R. F., Winter, L., & Soria, R. 2007, ApJ, 660, 580

Sun, W-H. & Malkan, M. A. 1989, ApJ, 346, 68

Swartz, D. A., Ghosh, K. K., McCollough, M. L., Pannuti, T. G., Tennant, A. F., & Wu, K. 2003, ApJS, 144, 213

Vierdayanti, K., Mineshige, S., Ebisawa, K, & Kawaguchi, T. 2006, PASJ, 58, 915

Winter, L. M., Mushotzky, R. F., & Reynolds, C. S. 2006, ApJ, 649, 730

Winter, L. M., Mushotzky, R. F., & Reynolds, C. S. 2007, ApJ, 655, 163

Table 1.   The Disk-Dominated ULX Sources

Ob ID	Galaxy	D (Mpc)	Object	RA (h m s)	Dec ($\circ$ $'$ $''$)	Tot. Red. Cts	Red. Ct. Rate (10^{-2} cts t^{-1})
0200980101	M81	3.6[1]	x1	09 55 32.9	+69 00 34.8	6913, 6524, -	9.12, 8.00, -
0104260101	M101	7.4[2]	x2	14 03 03.8	+54 27 37	874, 925, 1879	3.22, 3.04, 9.55
0152020101	NGC 253	3.73[3]	x1	00 47 32.8	-25 17 52.6	5874, 6316, 16454	8.78, 9.24, 28.46
			x3	00 47 35.2	-25 15 13.8	2266, 2360, 5089	3.33, 3.41, 8.72
			x4	00 47 23.3	-25 19 06.5	801, 736, 1659	1.16, 1.05, 2.82
0111240101	Circinus	4.0[4]	x2	14 12 54.2	-65 22 55.3	1391, -, 2703	1.51, -, 4.07

[1] Freedman et al. (1994).

[2] Kelson et al. (1996); Juvcevic & Butcher (2006).

[3] Calculated from the distance modulus given in NED. Also refer to Karachentsev et al. (2003); Rekola et al. (2005).

[4] Freeman et al. (1977); Iaria et al. (2005).

Table 2.   Fitting Results

Galaxy	Object	n_H[a]	$M/100\mathrm{M}_\odot$	L/L_e[b]	Spin[c]	Cos i[d]	χ^2/dof	L_{obs}/L_{bol}[e]
M81	x1	$1.90^{+0.12}_{-0.11}$	$0.73^{+0.12}_{-0.06}$	$1.00_{-0.15}$	$0.997_{-0.01}$	$0.53^{+0.03}_{-0.02}$	386.3/397	66.2/76.5
...	...	$1.61^{+0.11}_{-0.11}$	$0.49^{+0.25}_{-0.16}$	$0.82^{+0.40}_{-0.28}$	$0.999_{-0.05}$	$0.52^{+0.12}_{-0.18}$	392.6/397	-
M101	x2	$1.18^{+0.18}_{-0.33}$	$0.57^{+1.21}_{-0.47}$	$0.75^{+0.25}_{-0.47}$	$0.997_{-0.20}$	$0.59^{+0.15}_{-0.38}$	156.0/156	41.5/46.1
...	...	$0.96^{+0.18}_{-0.15}$	$0.63^{+1.27}_{-0.60}$	$0.38^{+6.11}_{-0.26}$	$0.999_{-2.0}$	$0.46^{+0.54}_{-0.37}$	157.6/156	-
NGC 253	x1	$1.68^{+0.12}_{-0.15}$	$0.72^{+0.09}_{-0.22}$	$0.45^{+0.11}_{-0.10}$	$0.997_{-0.12}$	$0.34^{+0.10}_{-0.04}$	998.5/963	29.2/31.5
...	...	$1.51^{+0.08}_{-0.10}$	$0.73^{+0.22}_{-0.19}$	$0.23^{+0.08}_{-0.05}$	$0.999_{-0.03}$	$0.28^{+0.09}_{-0.15}$	999.3/963	-
	x3	$2.93^{+0.15}_{-0.19}$	$0.50^{+0.31}_{-0.25}$	$0.20^{+0.19}_{-0.07}$	$0.997_{-0.20}$	$0.51^{+0.20}_{-0.17}$	379.6/388	10.1/11.0
...	...	$2.79^{+0.16}_{-0.13}$	$0.63^{+1.13}_{-0.31}$	$0.09^{+0.09}_{-0.06}$	$0.999_{-0.20}$	$0.42^{+0.28}_{-0.33}$	380.5/388	-
	x4	$0.64^{+0.21}_{-0.21}$	$0.23^{+0.68}_{-0.13}$	$0.14^{+0.10}_{-0.08}$	$0.997_{-0.34}$	$0.46^{+0.27}_{-0.42}$	143.9/140	3.0/3.4
...	...	$0.45^{+0.18}_{-0.27}$	$0.35^{+0.42}_{-0.30}$	$0.05^{+0.30}_{-0.03}$	$0.999^{+0.001}_{-2.0}$	$0.33^{+0.67}_{-0.25}$	145.4/140	-
Circinus	x2	$5.42^{+0.27}_{-0.38}$	$3.40^{+12.70}_{-3.30}$	$0.04^{+0.60}_{-0.01}$	$0.996^{+0.001}_{-1.0}$	$0.07^{+0.68}_{-0.07}$	176.4/173	7.3/8.6
...	...	$5.45^{+0.46}_{-0.36}$	$0.13^{+3.28}_{-0.01}$	$0.34^{+0.03}_{-0.33}$	$0.501^{+0.498}_{-1.5}$	$1.00^{+0.00}_{-0.91}$	177.6/173	-

[a] Column density in units of 10^{21} cm^{-2}.

[b] Luminosity normalized to the Eddington luminosity.

[c] Dimensionless spin parameter of the black hole.

[d] i - the inclination angle, i.e., the angle between the disk normal and the line of sight.

[e] The ratio of the observed luminosity to the model integrated luminosity. Luminosity is in units of 10^{38} erg s^{-1}

Note. — 1) For each object, the first row shows the fitting results from BHSPEC and the second row with "..." shows the results from KERRBB; 2) All uncertainties were computed with $\Delta\chi^2 = 2.706$, equivalent to 90% confidence for a single parameter. 3) Where no upper uncertainty is shown, the data are consistent with all parameters up to the edge of the parameter space, i.e., for L/L_E the upper bound is unity while for spin it is 0.997 for BHSPEC and 0.999 for KERRBB.
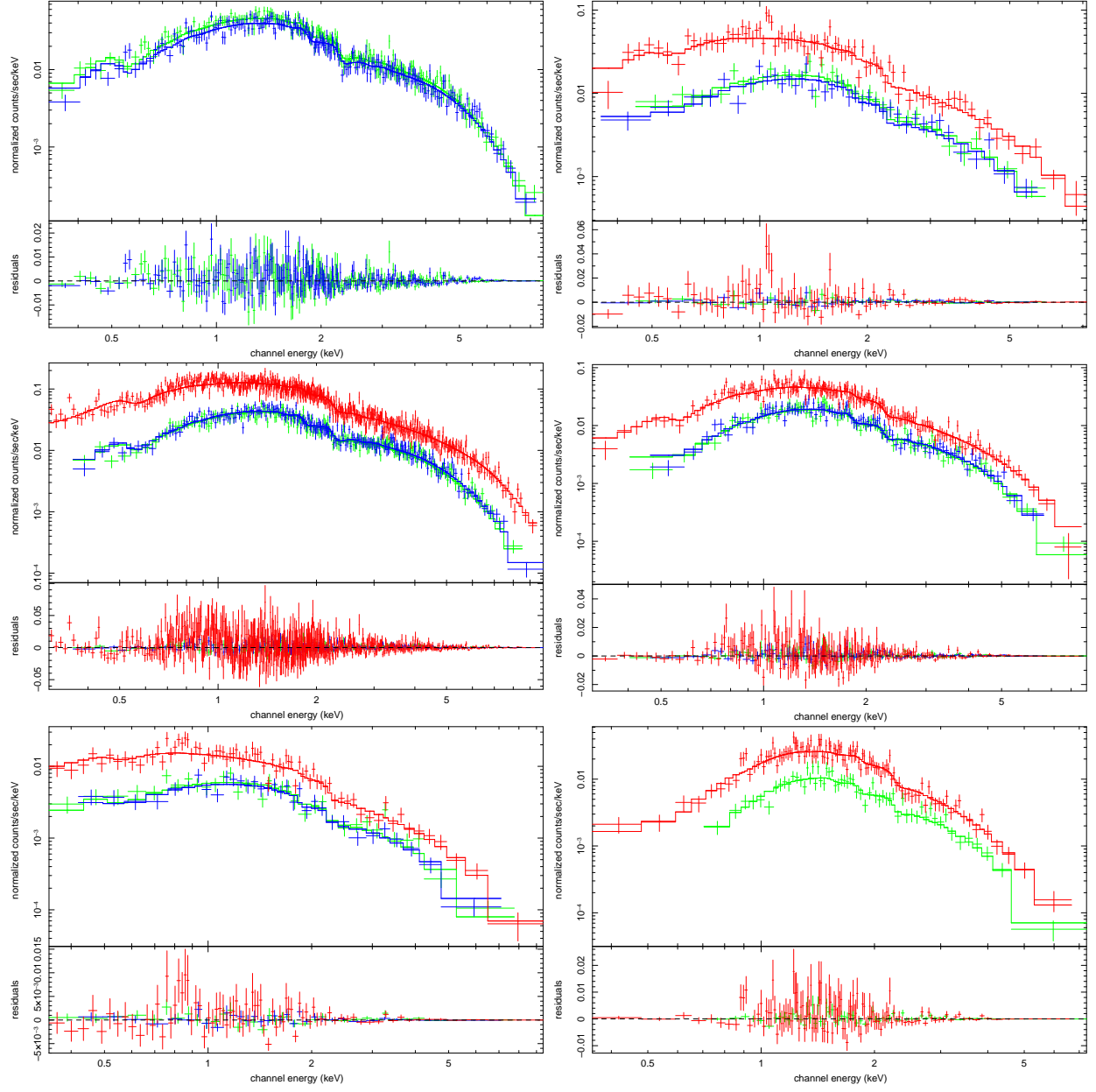
Fig. 1.— Observed spectra and best-fit models (only BHSPEC shown). Panels from top to bottom: upper left — M81 X1, upper right — M101 X1, middle left — NGC 253 X1, middle right — NGC 253 X3, lower left — NGC 253 X4, lower right — Circinus X2. In each panel, the green, blue and red colors represent the data from MOS1, MOS2 and PN, respectively.
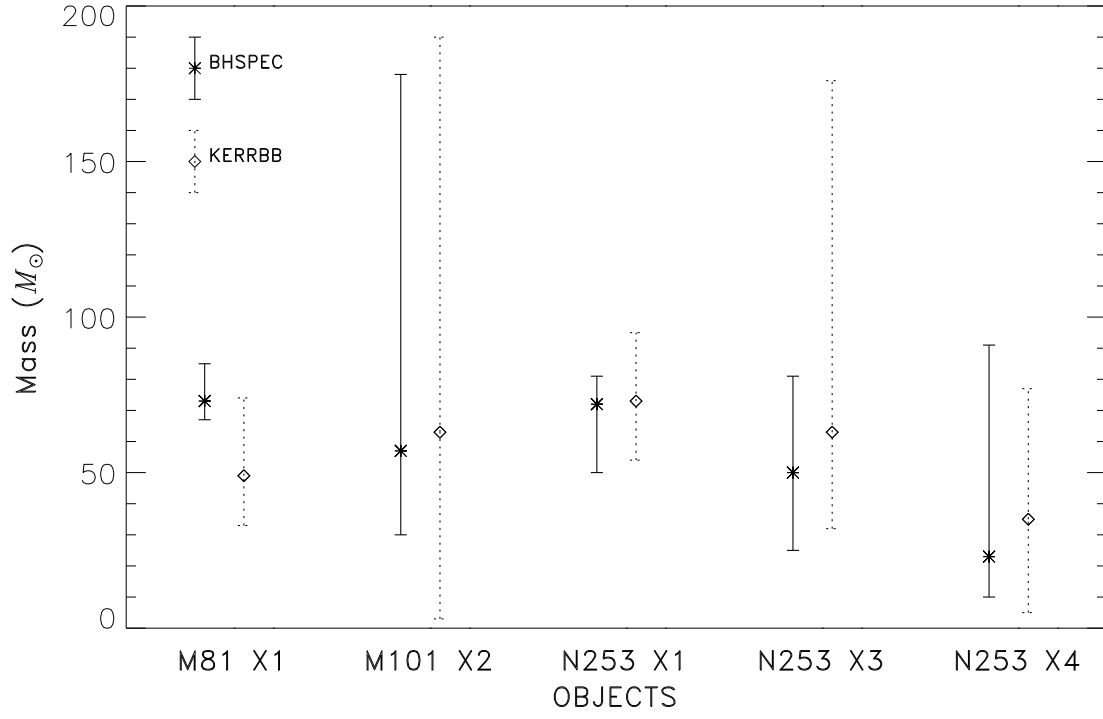
Fig. 2.— The distribution of black hole masses in our sample (except Circinus X2). Masses derived using BHSPEC are shown by stars, those inferred on the basis of KERRBB are shown with open diamonds. All uncertainties were computed with $\Delta\chi^2 = 2.706$, equivalent to 90% confidence for a single parameter.
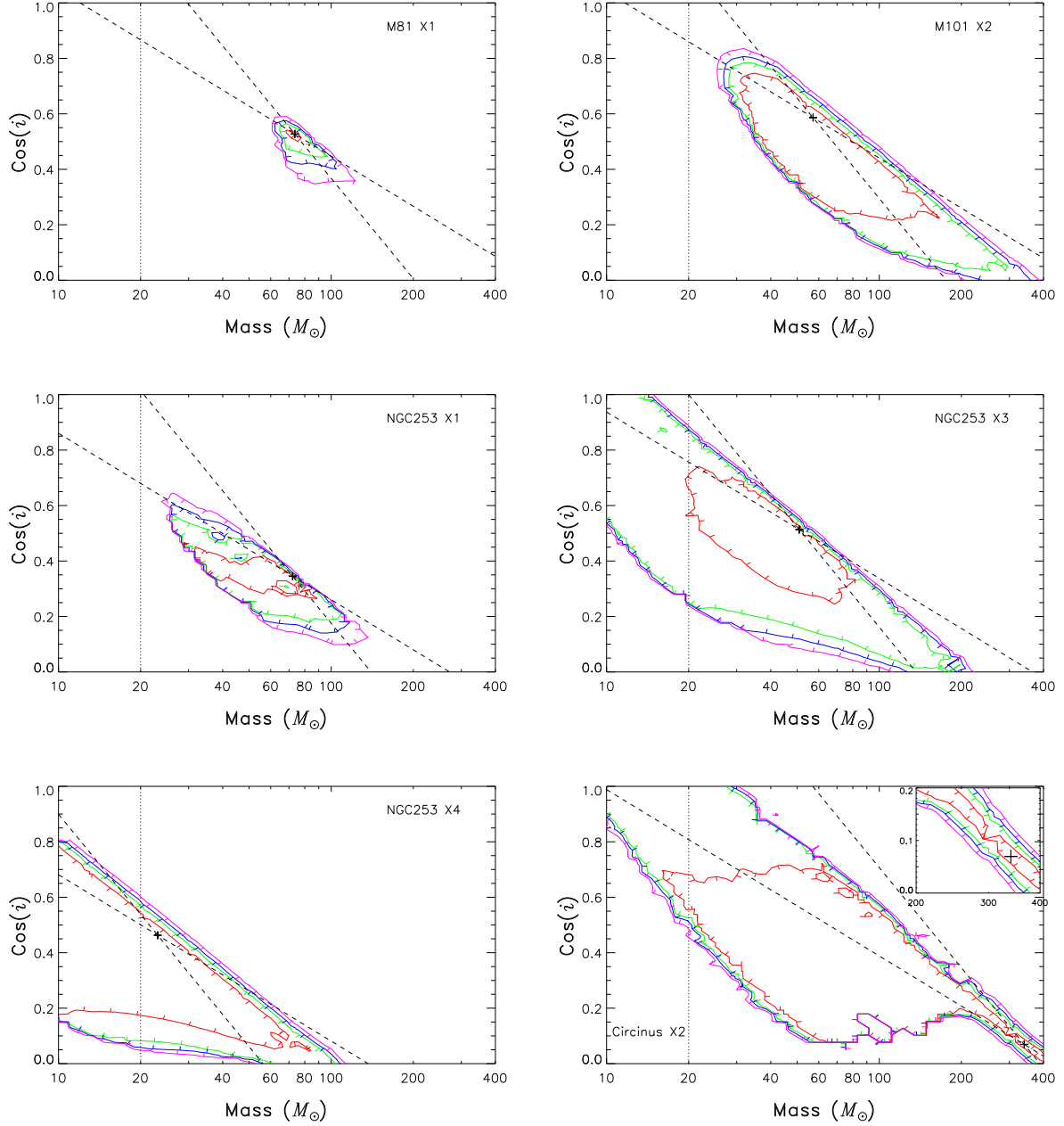
Fig. 3.— Confidence level contours in the M–$\cos i$ plane. The location of the least χ^2 is marked by a plus sign. A pair of dashed lines shows the extreme Kerr and Schwarzschild degeneracy relations suggested by Sun & Malkan (1989). A dotted vertical line at $M = 20 M_\odot$ marks the greatest mass consistent with any of the known Galactic black hole binaries (McClintock & Remillard 2004). The four contours show values of χ^2 above the minimum by $\Delta\chi^2 = 2.30$ (red), 6.14 (green), 9.21 (blue), 13.82 (magenta). These correspond to the 68.3% (1-σ), 95.4% (2-σ), 99.0% and 99.9% confidence levels, respectively. Short ticks along each contour show the "downhill" direction in χ^2.